ARTICLES
https://doi.org/10.1038/s41557-019-0312-z
nature chemistry

Formation of carbon–nitrogen bonds in carbon monoxide electrolysis

Matthew Jouny[1,6], Jing-Jing Lv[1,2,6], Tao Cheng[3,4,5,6], Byung Hee Ko[1], Jun-Jie Zhu[2], William A. Goddard III[3,4*] and Feng Jiao[1*]

The electroreduction of CO_2 is a promising technology for carbon utilization. Although electrolysis of CO_2 or CO_2-derived CO can generate important industrial multicarbon feedstocks such as ethylene, ethanol, *n*-propanol and acetate, most efforts have been devoted to promoting C–C bond formation. Here, we demonstrate that C–N bonds can be formed through co-electrolysis of CO and NH_3 with acetamide selectivity of nearly 40% at industrially relevant reaction rates. Full-solvent quantum mechanical calculations show that acetamide forms through nucleophilic addition of NH_3 to a surface-bound ketene intermediate, a step that is in competition with OH^- addition, which leads to acetate. The C–N formation mechanism was successfully extended to a series of amide products through amine nucleophilic attack on the ketene intermediate. This strategy enables us to form carbon–heteroatom bonds through the electroreduction of CO, expanding the scope of products available from CO_2 reduction.

Decarbonization of the chemical industry presents a considerable challenge in breaking our reliance on fossil resources and reducing CO_2 emissions[1–4]. Driven by the increasingly rapid deployment of renewable power generation[5], the cost of renewable electricity has decreased considerably, making electrochemical CO_2 reduction an attractive approach to produce sustainable fuels and chemicals[6–8]. Multi-carbon (C_{2+}) chemicals are desirable products because they are more valuable than typical single-carbon products such as CO (refs. [6,9,10]). Highly alkaline electrolytes are often used to enhance C_{2+} selectivity; however, the inevitable reaction of OH^- ions with CO_2 to form undesired carbonates at the electrode–electrolyte interface disrupts the electrolysis process[11,12]. This problem can be addressed through a two-step process in which CO_2 is first reduced to CO electrochemically at non-alkaline conditions, which is followed by a CO reduction step to produce C_{2+} chemicals in alkaline environments. Regardless of CO_2 or CO reduction, only four major C_{2+} products—ethylene, acetate, ethanol and *n*-propanol—have been reported in aqueous electrolytes[13–19]. Although these products are of importance in current chemical industries, the ability to produce chemicals beyond simple carbon species is critically important because valuable specialty chemicals often contain heteroatoms[20,21].

In a recent study, we observed an enhanced acetate selectivity in CO reduction in comparison with CO_2 reduction under identical conditions[22]. Surface pH calculations and isotopic labelling studies suggested that acetate was favourably formed through nucleophilic attack of OH^- on a ketene-like intermediate under highly alkaline conditions, which is in good agreement with a previous study by Kanan et al.[13]. As ketene is known to be highly reactive with nucleophilic agents, it is reasonable to assume that the ketene-like intermediate present on the Cu catalyst surface in CO reduction could readily react with other nucleophilic agents besides OH^- ions. We postulated that if a nitrogen-containing nucleophilic agent such as NH_3 was introduced to the Cu-catalysed CO electrolysis system, a carbon–nitrogen bond could be formed. The overall strategy for C–N bond formation is outlined in Fig. 1a.

Here, we report C–N bond formation that results from CO electroreduction in the presence of NH_3. An electrochemical production of acetamide with nearly 40% Faradaic efficiency was achieved at a current density of 300 mA cm^{-2}. Our previous full-solvent quantum mechanical calculations[23,24] revealed that—under neutral or basic conditions—the reaction mechanism involves CO dimerization and sequential transfer of H from two surface waters to form the *(HO)C=COH intermediate that subsequently proceeds through two separate pathways to form C_2H_4 and ethanol/*n*-propanol. We show now that *(HO)C=COH is also hydrolysed to *C=C=O, which in turn reacts with NH_3 to form intermediates that proceed to form acetamide while suppressing the formation of other C_{2+} products. We also successfully extended the range of C–N containing products to *N*-methylacetamide, *N*-ethylacetamide, *N*,*N*-dimethylacetamide, acetic monoethanolamide and aceturic acid. Our results provide critical mechanistic insights into Cu-catalysed CO_2/CO electroreduction and demonstrate the construction of carbon–heteroatom bonds in CO_2/CO electrolysis.

Results and discussion

The concept of a nucleophilic NH_3 addition during CO electrolysis was verified through a series of electrolysis experiments using a three-compartment continuous flow cell with a well-defined triple-phase interface (Supplementary Fig. 1). Copper cathodes were prepared by coating Cu nanoparticles (NPs) onto a gas diffusion layer (GDL). The size distribution and monoclinic phase of the Cu NPs were characterized using scanning electron microscopy (SEM), X-ray diffraction (XRD) and X-ray photoelectron spectroscopy (XPS) (Supplementary Fig. 2). The Cu NPs are mainly highly crystalline metallic Cu with an average particle size of 50 ± 20 nm, but they also contain a small fraction of Cu oxides. The electroreduc-

[1]Center for Catalytic Science and Technology, Department of Chemical and Biomolecular Engineering, University of Delaware, Newark, DE, USA. [2]State Key Laboratory of Analytical Chemistry for Life Science, School of Chemistry and Chemical Engineering, Nanjing University, Nanjing, China. [3]Joint Center for Artificial Photosynthesis, California Institute of Technology, Pasadena, CA, USA. [4]Materials and Process Simulation Center, California Institute of Technology, Pasadena, CA, USA. [5]Institute of Functional Nano & Soft Materials, Jiangsu Key Laboratory for Carbon-based Functional Materials & Devices, Joint International Research Laboratory of Carbon-based Functional Materials and Devices, Soochow University, Suzhou, Jiangsu, China. [6]These authors contributed equally: Matthew Jouny, Jing-Jing Lv, Tao Cheng. *e-mail: wag@caltech.edu; jiao@udel.edu

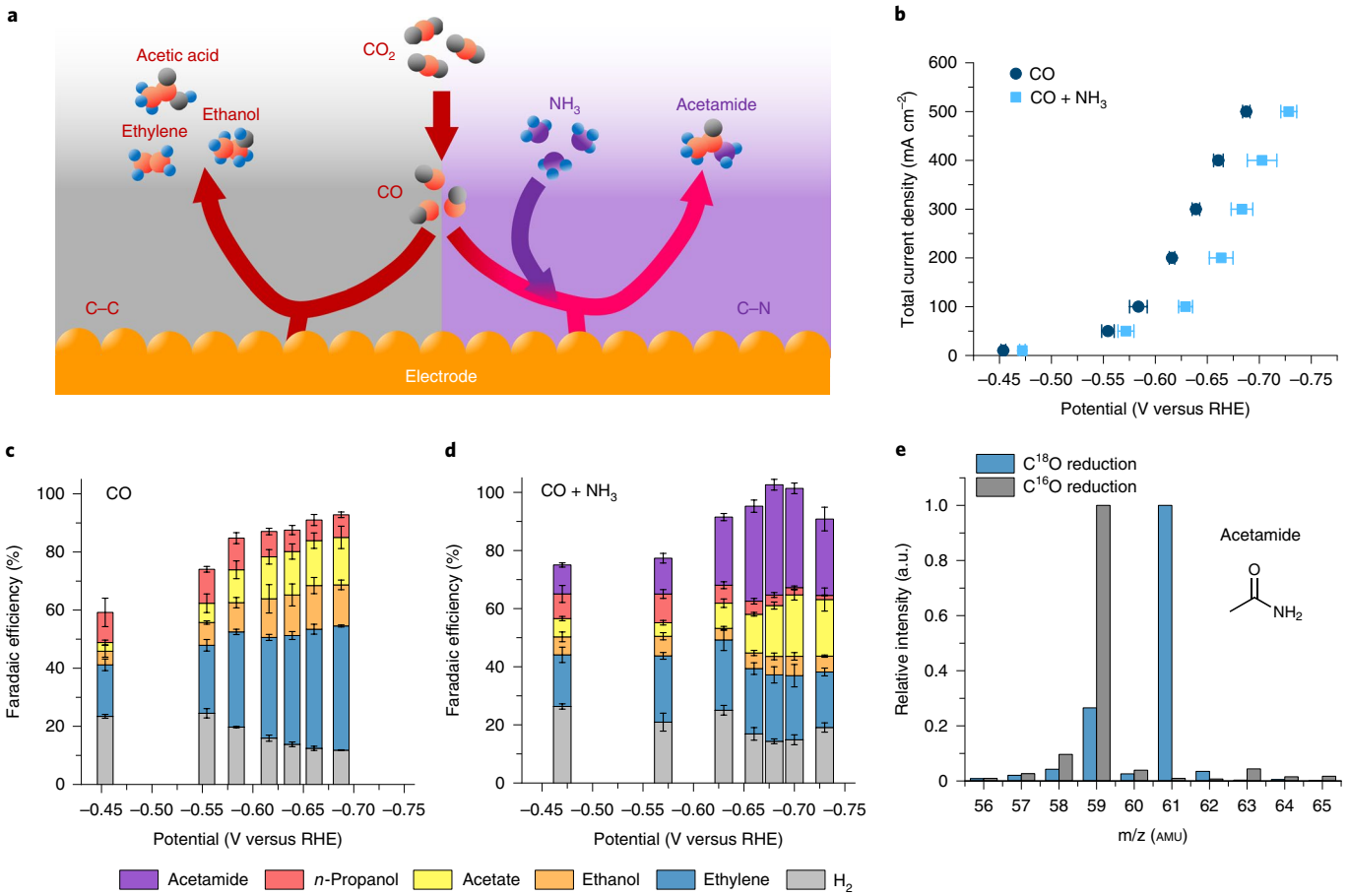

Fig. 1 | Acetamide production from CO electrolysis with NH_3. **a**, A schematic that depicts NH_3 inducing C–N bond formation from CO electrolysis. **b**, Electrode polarization curves for electrolysis in 1 M KOH under pure CO gas and a NH_3/CO ratio of 2:1. **c**,**d**, The Faradaic efficiencies versus the applied potential for CO (**c**) and CO + NH_3 (**d**). **e**, A mass spectrum comparing acetamide produced from $C^{16}O$ and $C^{18}O$. The error bars represent the s.d. for at least three independent measurements.

tion activity of CO was measured through steady-state galvanostatic electrolysis in a 1 M KOH electrolyte. Under a pure CO gas feed, a near-exponential polarization response was observed (Fig. 1b, Supplementary Table 1), with up to ~80% C_{2+} products for a total current density of 500 mA cm^{-2}. The major CO electroreduction products observed were ethylene, ethanol, acetate and *n*-propanol (Fig. 1c).

After establishing the baseline of CO electrolysis activity, NH_3 gas was fed together with CO in an NH_3:CO (mol/mol) ratio of 2:1. In the presence of NH_3 gas, the required potential to achieve the same current density increased by ~30 mV (Fig. 1b, Supplementary Table 1), possibly due to the reduced CO partial pressure in the flow cell[25,26]. Remarkably, the presence of NH_3 led to considerable production of acetamide, with a Faradaic efficiency up to 38% and a partial current density of 114 mA cm^{-2} at −0.68 V versus the reversible hydrogen electrode (RHE). Furthermore, the observed amounts of ethylene and alcohols were greatly decreased at moderate to high overpotentials, whereas acetate selectivity was maintained (Fig. 1d). Increasing the fraction of CO in the gas feed shifted selectivity towards pure CO reduction products, but increasing the ratio of NH_3 beyond 2:1 did not significantly influence the acetamide selectivity (Supplementary Fig. 3). Similar results were obtained using a mixture of ammonium hydroxide and KOH or KCl as the catholyte together with a pure CO gas feed (Supplementary Fig. 4). This suggests that acetamide can form in both gas and liquid phase NH_3 with appreciable Faradaic efficiency. To evaluate the stability of the Cu-catalysed CO electrolysis process in the presence of NH_3, an eight hour continuous experiment was performed at a total current density of 100 mA cm^{-2} that led to stable production of acetamide (Supplementary Fig. 5 and Supplementary Table 1). The spent Cu catalyst was characterized by SEM, XRD and XPS and no visible change was observed in the morphology and structure after electrolysis (Supplementary Fig. 6). X-ray photoelectron spectroscopy revealed some Cu oxides following electrolysis, which is probably due to exposure to air, as recent studies[27,28] have shown that Cu catalysts are fully metallic while under reducing potentials. This is further supported by in situ X-ray absorption spectroscopy performed on a 5-nm-thick Cu catalyst[29] in 5 M ammonium hydroxide showing entirely Cu^0 features (Supplementary Fig. 7). Furthermore, significant amounts of acetamide were also produced on other Cu-based catalysts (Supplementary Fig. 8), suggesting that the formation of acetamide is universal in Cu-catalysed CO electrolysis in the presence of NH_3. The use of CO_2 as the feed gas resulted in spontaneous carbonate formation and the observation of no amides, indicating this chemistry may be difficult through direct CO_2 reduction (Supplementary Fig. 9).

These experimental results strongly suggest that a surface ketene intermediate is probably formed on the Cu catalyst surface during CO electroreduction and nucleophilically attacked by either OH^- or NH_3 to form acetate or acetamide, respectively, under highly

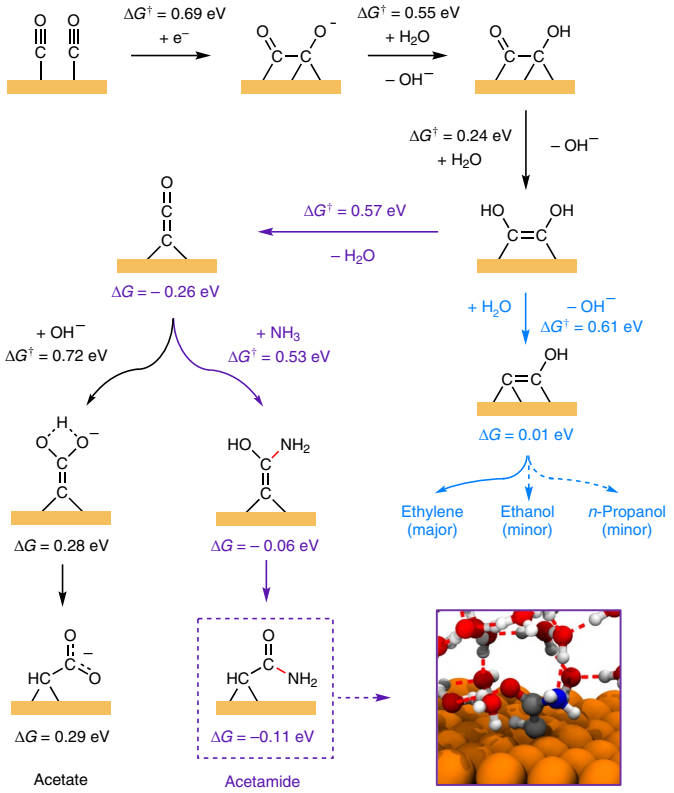

Fig. 2 | The mechanism for CO reduction on Cu that shows how it splits at [*(HO)C=COH] into two pathways. One pathway features *C=COH (and produces ethylene, ethanol and *n*-propanol) whereas the other features *C=C=O (and produces acetamide and acetate). The inset shows the structure of *CH-C(=O)NH_2, the second reactive intermediate with a C-N bond.

alkaline environments. This is further supported by a shift in selectivity from amide to acetate for CO electrolysis with NH_3 in electrolytes with increasing KOH concentration (Supplementary Fig. 10). Furthermore, because the ketene intermediate contains one oxygen originated from CO, the resulting acetate should contain two oxygen atoms with one from CO and the other from water, which is in good agreement with recent studies[22,30]. In the case of a nucleophilic attack by NH_3, the oxygen in acetamide should originate from CO. We verified the origin of oxygen in acetamide by conducting a $C^{18}O$ isotopic labelling study, where ^{18}O labelled acetamide was the dominant product (Fig. 1e), consistent with the proposed ketene mediated reaction mechanism.

To further elucidate the reaction mechanism, we used quantum mechanics (QM; Perdew–Burke–Ernzerhof D3 (PBE-D3) density functional theory) to investigate the electrocatalytic formation of acetamide in the presence of NH_3 (see the Supplementary Information for simulation details). We used the full-solvent methods previously applied to CO_2 reduction[23] and CO reduction on Cu(100), which is the dominant Cu surface under our conditions and the most active for C–C coupling[24,30,31]. The explicit solvation calculations have been demonstrated to be robust considering that simulations from the independent work of Bagger et al.[32] reached very similar conclusions as our previous work. Our earlier QM full-solvent calculations showed[24,31] that under neutral or basic conditions the reaction mechanism involves CO dimerization and sequential transfer of H from two surface water to form *(HO)C=COH with an overall free energy barrier ($\Delta G^{\ddagger}$) at 298 K of 0.69 eV. This then leads to *C=COH with $\Delta G^{\ddagger}$ = 0.61 eV that subsequently goes through two separate pathways to form C_2H_4 (65%) and ethanol/*n*-propanol (35%).

Now we consider a new step starting with *(HO)C=COH. We find $\Delta G^{\ddagger}$ = 0.57 eV to form *C=C=O through a water-mediated pathway. The possibility of the *C=C=O intermediate was first proposed by Koper[33], which was postulated as an intermediate in the ethylene pathway. However, later full-solvent QM showed that the formation of C_2H_4 derives from *C=COH as in Fig. 2. Our new QM calculations find that *C=C=O derives from dehydration of *(HO)C=COH. Thus, in the competition with *C=COH from proton-coupled electron transfer, *C=C=O prefers high pH and less negative potential. This is consistent with the experimental observation of exclusive acetate formation on Cu NP at pH 14 and –0.25 V versus RHE[34].

We find that C–N bond formation arises from NH_3 reacting with *C=C=O to form *C=C(OH)NH_2 ($\Delta G^{\ddagger}$ = 0.53 eV) via a water-mediated reaction pathway. We then discover that *C=C(OH)NH_2 isomerizes into *CH–C(=O)NH_2 through a keto–enol tautomerism that is exergonic by –0.11 eV. These two reactions are not electrochemical and *CH–C(=O)NH_2 remains a 2e⁻ intermediate just as it did for *C=C=O. The subsequent steps involve two proton-coupled electron transfers to the acetamide product as shown in Fig. 2. In competition with NH_3 addition to *C=C=O, we find that acetate forms through direct reaction of OH^- with *C=C=O to form *C=C(OH)O^- ($\Delta G^{\ddagger}$ = 0.72 eV), which then undergoes a similar keto–enol tautomerism and a subsequent proton-coupled electron transfer. The presence of K^+ will stabilize *C=C(OH)O^- on the catalyst surface.

With these insights, we can extend the reaction networks of CO reduction to ethylene[24] and ethanol[24,30] to include the branches of acetamide and acetate from NH_3 and OH^- addition, respectively (Fig. 2). The observed suppression of ethylene and alcohols in the presence of high concentrations of NH_3 (Fig. 1c,d) is probably due to decreased water availability hindering protonation of *(HO)C=COH to form *C=COH, which results in an overall increase in *C=C=O formation. Although acetamide formation from *C=C=O is more energetically favourable than acetate formation, acetate production is maintained at high current densities as OH^- is generated directly at the catalyst surface.

As the key intermediate towards acetate and acetamide in Cu-catalysed CO electroreduction, ketene is also known to be highly reactive with other amine-type nucleophilic agents. We therefore investigated Cu-catalysed CO electrolysis in the presence of additional amines in hope of producing the corresponding amides. We performed electroreduction of a pure CO gas feed using 5 M solutions of methylamine, ethylamine and dimethylamine that contain 1 M KCl as the supporting electrolyte. We used 1 M KCl to enhance the ionic conductivity of the electrolytes. As shown in Fig. 3a–c, analogous results to the CO/NH_3 system were obtained, where substantial amounts of *N*-methylacetamide, *N*-ethylacetamide and *N*,*N*-dimethylacetamide were produced at high total current densities of up to 300 mA cm^{-2} with peak Faradaic efficiencies of 42%, 34% and 36%, respectively (Supplementary Table 2). The formation of these amides was confirmed using mass and ^1H NMR spectrometry (Supplementary Figs. 11 and 12).

The molar fraction of each C_{2+} product (excluding hydrogen) at 200 mA cm^{-2} in each amine system is shown in Fig. 3d. Data for pure CO electrolysis were also shown for comparison. Similar to NH_3, the molar fractions for ethylene and ethanol decrease by about twofold and fourfold, respectively, for all amines tested. The trend of the amide molar fraction across various amines is opposite to that of acetate and correlates well with the reactivity (or nucleophilicity) of the precursor amino group. The reactive N–H bond is weakest for dimethylamine and strongest for NH_3, with methylamine and ethylamine between[35]. As the amine competes with OH^- to react with the ketene intermediate, it is reasonable that dimethylamine produces the highest ratio of amide to acetate, whereas NH_3 produces the lowest. Therefore, these observations further support the

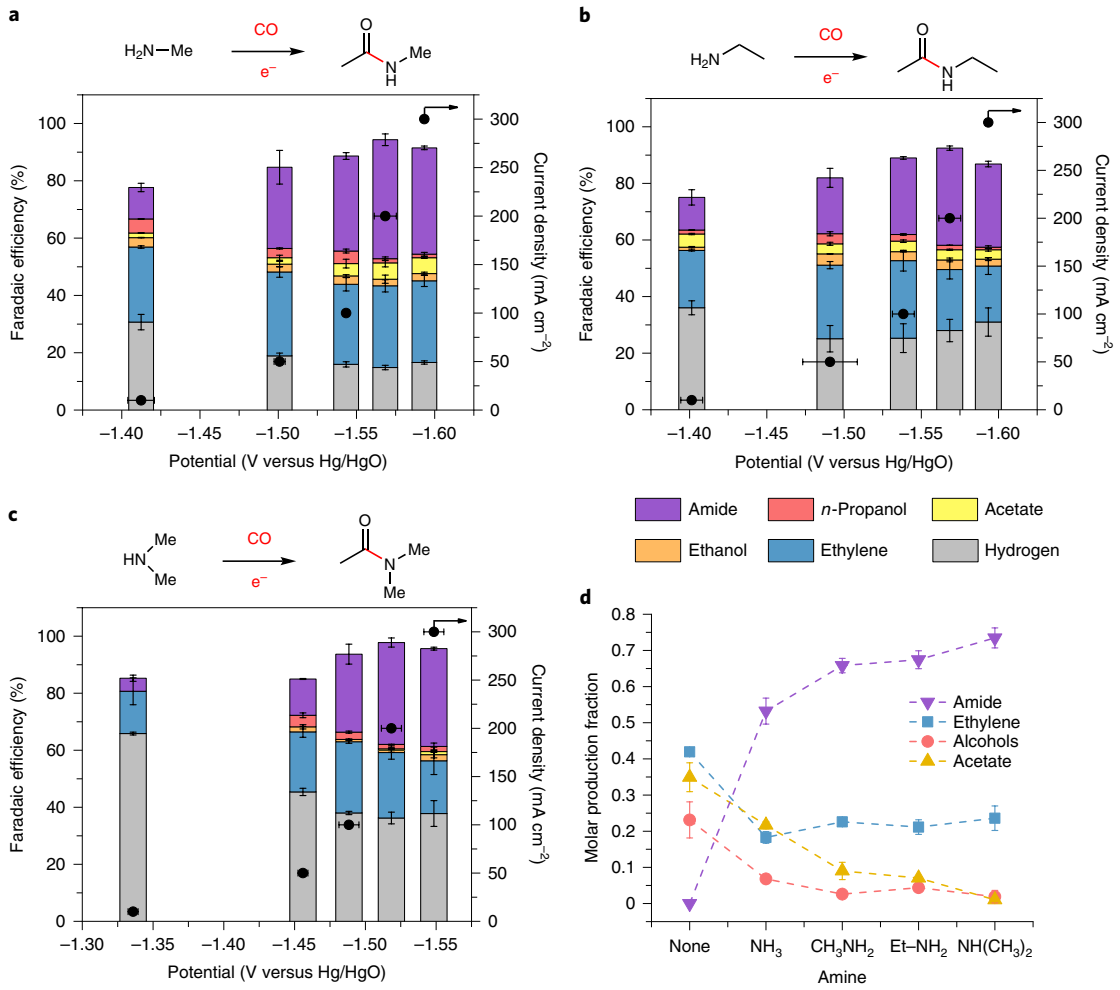

Fig. 3 | Electrochemical production of longer amides from CO electrolysis in 5 M amine solutions. a–c, The total current density and Faradaic efficiencies for CO electrolysis in 1 M KCl solution containing (**a**) 5 M methylamine, (**b**) 5 M ethylamine and (**c**) 5 M dimethylamine. **d**, The molar production fraction for different C_{2+} products excluding hydrogen at 200 mA cm^{-2} for CO reduction with various amines. Note that the NH_3 fractions are calculated from Fig. 1d. The error bars represent the s.d. for at least three independent measurements.

mechanism proposed earlier and provide important mechanistic insight into the Cu-catalysed CO electroreduction reaction.

We were also able to further extend the range of products to acetamides that contain hydroxyl and carboxylate functional groups. Acetic monoethanolamide and aceturic acid were produced by performing CO electrolysis in solutions of ethanolamine and glycine, respectively (Supplementary Fig. 13). As these products contain reactive functional groups, they can be used as potential precursors to build larger molecules with higher values. This opens up a wide library of chemical transformations in which CO electrolysis can play an important role. Although the goal of this work is to demonstrate the concept of electrochemical C–N bond formation, future studies can identify and optimize the production of more species.

Conclusion

In summary, we demonstrate a new route to produce a variety of acetamides through CO electrolysis at ambient conditions. These products are commonly used in the polymer and pharmaceutical industries[20,36]. In particular, *N*,*N*-dimethylacetamide has substantial usage as a polymerization solvent, and currently requires harsh synthesis conditions[37]. Although the amines used in this work are currently produced with methane-derived NH_3 and methanol, renewable NH_3 synthesis is currently an area of great interest and many promising production routes have been demonstrated recently[38–40]. More importantly, the concept of nucleophilic attack of a ketene intermediate in Cu-catalysed CO electroreduction enables the formation of a much wider range of chemicals containing carbon–heteroatom bonds that cannot be built in conventional CO electrolysis processes. The ability to produce heteroatom-containing carbon species would greatly increase the potential of CO_2/CO electrolysis technologies for commercial applications.

Methods

Materials characterization. All chemicals were of analytical grade and used as received without further purification unless otherwise noted. Commercial Cu NPs with 25 nm diameter and Cu particles with 1 μm diameter were used as catalysts in this work (both purchased from Sigma Aldrich). The microstructures of the catalysts were characterized by field emission SEM (Auriga, 1.5 kV). Powder XRD measurements were conducted on a D8 ADVANCE X-ray diffractometer (Bruker). A Thermo Scientific K-Alpha XPS system was used and XPS fitting was conducted by CasaXPS software with the adventitious carbon peak being calibrated to 284.8 eV. All peaks were fitted using a Gaussian/Lorentzian product line shape and a Shirley background.

Flow cell electrolysis. Electrochemical measurements were conducted on an Autolab potentiostat (PG128N) in a three-electrode system. Unless otherwise noted, an IrO_2 (Alfa Aesar) coated GDL (Sigracet 29 BC, Fuel Cell Store) with a loading of 0.5 mg cm^{-2} was used as the counter electrode, whereas Ag/AgCl (saturated KCl, Pine Research) or Hg/HgO (filled with 1 M KOH, Pine Research) were used as the reference electrodes. The Cu NPs (or the Cu-coated GDL) were applied as the working electrode, which was prepared by hand painting a catalyst

ink. We weighed the GDL before and after deposition to record its actual catalyst loading and kept all of the electrodes with a loading of 0.6 mg cm^{-2}. To prepare the catalyst ink, 25 mg of catalyst was ultrasonically dispersed in the mixture of 3 ml of isopropanol, 500 µl of multi-walled carbon nanotube solution (5 mg multi-walled carbon nanotube (>98%, Sigma-Aldrich) dispersed in 5 ml THF) and 20 µl of Nafion (10 wt% aqueous solution, Fuel Cell Store). The mixture was then sonicated for 30 min before dropcasting.

The electrolysis experiments were performed in a three-channel flow cell with channels with dimensions of 2×0.5×0.15 cm^3. The electrode area was 1 cm^2 and the electrode to membrane distance was 1.5 mm. An external Ag/AgCl or Hg/HgO reference electrode located ~5 cm from the cathode was used to measure the cathodic half-cell potential. Electrolysis measurements were performed through chronopotentiometry using an Autolab PGSTAT128N potentiostat/galvanostat. All of the potential measurements were converted to the RHE using the following formula: $E_{RHE} = E_{Ag/AgCl} + 0.222 + 0.059 \times pH$ (in volts) or $E_{RHE} = E_{Hg/HgO} + 0.097 + 0.059 \times pH$ (in volts), where the standard values for the reference electrodes were found by calibration through cyclic voltammetry in a H_2-saturated 1 M KOH electrolyte with a Pt cathode and anode. The measured pH values of bulk electrolyte exiting the flow cell—obtained using a pH meter (Apera Instruments)—were used for the RHE conversions unless stated otherwise. The measured potential was iR corrected at 100% by measuring the solution resistance between the reference electrode and cathode with the current-interrupt technique before each applied current[41]. The device is fabricated from acrylic and includes the gas channel for the following: feeding CO and NH_3; anode and cathode channels for the flowing electrolyte; an anion exchange membrane (FAA-3, Fumatech) for separating the anode and cathode; and solid acrylic end pieces. Polytetrafluoroethylene gaskets were placed between each component for sealing and the device was tightened using six bolts. The CO flow rate was set via a mass flow controller (Brooks GF40) and the NH_3 flow rate was controlled by a rotameter (Cole Parmer, PMR1-010286). The electrolyte flow rates were controlled via a peristaltic pump (Cole Parmer), with the catholyte and anolyte flow rates set to 0.5 ml min^{-1} and 1 ml min^{-1}, respectively. Amines were scrubbed from the effluent gas from the flow cell using an acid trap (3 M H_2SO_4 solution) before entering the gas chromatograph.

For CO electrolysis in the presence of NH_3, the gas channel was co-fed with CO and NH_3, with 1 M KOH used as the catholyte and anolyte (Ag/AgCl reference electrode). For CO electrolysis in the presence of liquid phase amines, a pure CO gas feed was used, with the catholyte comprising the reactants (NH_3 H_2O, CH_3NH_2, $CH_3CH_2NH_2$, CH_3NHCH_3, $HOCH_2CH_2NH_2$ and NH_2CH_2COOH) and a supporting electrolyte (KOH or KCl), and a 1 M KOH anolyte (Hg/HgO reference electrode). A NiFe/Ni foam anode—prepared following a previously reported method[42]—was used as the anode electrode for the acetamide production stability test.

Product quantification. Gas products were quantified on a Multigas no. 5 GC (SRI Instruments) equipped with Hayesep D and Molsieve 5 Å columns leading to a thermal conductivity detector and a Hayesep D column leading to a flame ionization detector. Hydrogen was quantified using the thermal conductivity detector whereas ethylene and methane were detected using both a flame ionization detector and a thermal conductivity detector. The Faradaic efficiency for the products was calculated using the following equation:

$$\text{Faradaic efficiency } (\%) = \frac{nFxV}{j_{tot}} * 100$$

where n is the number of electrons transferred, F is Faraday's constant, x is the mole fraction of product, V is the total molar flow rate of gas and j_{tot} is the total current.

Liquid products were quantified using ^{1}H NMR (Bruker AVIII 600 MHz). The ^{1}H NMR spectra were obtained using a pre-saturation method for water suppression. Typically, 500 µl of collected diluted catholyte was mixed with 100 µl of internal standard solution (25 ppm (m/m) dimethyl sulfoxide (≥99.9%, Alfa Aesar) or 250 ppm (m/m) phenol (≥99%, Sigma-Aldrich) in D_2O). The electrochemical reactions for amide formation are provided in Supplementary Table 3. Amide production was further verified by GC–MS (gas chromatography–mass spectrometry) (Agilent 59771 A). The GC–MS spectral features were determined by comparing the mass fragmentation patterns with those of the National Institute of Standards and Technology library.

C^{18}O electrolysis. The labelled isotope experiment was performed by using labelled C^{18}O gas (95 at% ^{18}O, Sigma Aldrich) for electrolysis. The C^{18}O was extracted by a 30 ml syringe and was injected into the flow cell at 5 ml min^{-1} by a syringe pump, along with NH_3 at a flow rate of 10 ml min^{-1}. Electrolysis was conducted at a constant current of 200 mA cm^{-2} for 5 min and the catholyte was collected for analysis by GC–MS.

Model and methods. Electronic structure calculations were performed within the density functional theory framework, as implemented in the Vienna ab initio simulation program (a plane-wave pseudopotential package). The exchange and correlation energies were calculated using the PBE functional within the generalized gradient approximation. Spin polarization did not have an appreciable effect on the overall energies. The PBE-D3 method was employed to correct for the van der Waals interactions of water–water and water–Cu. We simulated the water–Cu(100) interface using 48 explicit water molecules (five layers, 1.21 nm thick) on a 4×4 Cu(100) surface slab (three layers) with an area of 1.02 nm^2. For the cases that involve NH_3, we also included the explicit NH_3 in our calculation along with 47 H_2O. The simulation protocol of free-energy calculations is the same as in our previous work[24]. To confirm the robustness of the calculation, the onset potential for the hydrogen evolution reaction on Cu(100) was predicted to be −0.4 V versus RHE, which is close to the experimental value[43]. More simulation details are included in the Supplementary Information.

Data availability

The datasets generated during and/or analysed during the current study are available from the corresponding author on reasonable request.

Code availability

The computational codes used in the current study are available from the corresponding author on reasonable request.

Received: 21 January 2019; Accepted: 10 July 2019;
Published online: 23 August 2019

References

1. Otto, A., Grube, T., Schiebahn, S. & Stolten, D. Closing the loop: captured CO_2 as a feedstock in the chemical industry. *Energy Environ. Sci.* **8**, 3283–3297 (2015).
2. Schiffer, Z. J. & Manthiram, K. Electrification and decarbonization of the chemical industry. *Joule* **1**, 10–14 (2017).
3. Katelhon, A., Meys, R., Deutz, S., Suh, S. & Bardow A. Climate change mitigation potential of carbon capture and utilization in the chemical industry. *Proc. Natl Acad. Sci. USA* **116**, 11187–11194 (2019).
4. Montoya, J. H. et al. Materials for solar fuels and chemicals. *Nat. Mater.* **16**, 70–81 (2016).
5. Haegel, N. M. et al. Terawatt-scale photovoltaics: transform global energy. *Science* **364**, 836–838 (2019).
6. De Luna, P. et al. What would it take for renewably powered electrosynthesis to displace petrochemical processes? *Science* **364**, eaav3506 (2019).
7. Verma, S., Lu, S. & Kenis, P. J. A. Co-electrolysis of CO_2 and glycerol as a pathway to carbon chemicals with improved technoeconomics due to low electricity consumption. *Nature Energy* **4**, 466–474 (2019).
8. Nitopi, S. et al. Progress and perspectives of electrochemical CO_2 reduction on copper in aqueous electrolyte. *Chem. Rev.* **119**, 7610–7672 (2019).
9. Jouny, M., Luc, W. & Jiao, F. General techno-economic analysis of CO_2 electrolysis systems. *Ind. Eng. Chem. Res.* **57**, 2165–2177 (2018).
10. Gao, D., Arán-Ais, R. M., Jeon, H. S. & Roldan Cuenya, B. Rational catalyst and electrolyte design for CO_2 electroreduction towards multicarbon products. *Nat. Catal.* **2**, 198–210 (2019).
11. Dinh, C.-T. et al. CO_2 electroreduction to ethylene via hydroxide-mediated copper catalysis at an abrupt interface. *Science* **360**, 783 (2018).
12. Verma, S. et al. Insights into the low overpotential electroreduction of CO_2 to CO on a supported gold catalyst in an alkaline flow electrolyzer. *ACS Energy Lett.* **3**, 193–198 (2018).
13. Li, C. W., Ciston, J. & Kanan, M. W. Electroreduction of carbon monoxide to liquid fuel on oxide-derived nanocrystalline copper. *Nature* **508**, 504–507 (2014).
14. Verdaguer-Casadevall, A. et al. Probing the active surface sites for CO reduction on oxide-derived copper electrocatalysts. *J. Am. Chem. Soc.* **137**, 9808–9811 (2015).
15. Bertheussen, E. et al. Acetaldehyde as an intermediate in the electroreduction of carbon monoxide to ethanol on oxide-derived copper. *Angew. Chem. Int. Ed.* **55**, 1450–1454 (2016).
16. Garza, A. J., Bell, A. T. & Head-Gordon, M. Mechanism of CO_2 reduction at copper surfaces: pathways to C_2 products. *ACS Catal.* **8**, 1490–1499 (2018).
17. Pang, Y. et al. Efficient electrocatalytic conversion of carbon monoxide to propanol using fragmented copper. *Nat. Catal.* **2**, 251–258 (2019).
18. Zhuang, T.-T. et al. Copper nanocavities confine intermediates for efficient electrosynthesis of C3 alcohol fuels from carbon monoxide. *Nat. Catal.* **1**, 946–951 (2018).
19. Zhang, H., Li, J., Cheng, M.-J. & Lu, Q. CO electroreduction: current development and understanding of Cu-based catalysts. *ACS Catal.* **9**, 49–65 (2018).
20. Pattabiraman, V. R. & Bode, J. W. Rethinking amide bond synthesis. *Nature* **480**, 471–479 (2011).
21. Nagib, D. Nitrogen gets radical. *Nat. Chem.* **11**, 396–398 (2019).
22. Jouny, M., Luc, W. & Jiao, F. High-rate electroreduction of carbon monoxide to multi-carbon products. *Nat. Catal.* **1**, 748–755 (2018).
23. Cheng, T., Xiao, H. & Goddard, W. A. Reaction mechanisms for the electrochemical reduction of CO_2 to CO and formate on the Cu(100) surface at 298 K from quantum mechanics free energy calculations with explicit water. *J. Am. Chem. Soc.* **138**, 13802–13805 (2016).

24. Cheng, T., Xiao, H. & Goddard, W. A. Full atomistic reaction mechanism with kinetics for CO reduction on Cu(100) from ab initio molecular dynamics free-energy calculations at 298 K. *Proc. Natl Acad. Sci. USA* **114**, 1795–1800 (2017).
25. Kim, B., Ma, S., Molly Jhong, H.-R. & Kenis, P. J. A. Influence of dilute feed and pH on electrochemical reduction of CO_2 to CO on Ag in a continuous flow electrolyzer. *Electrochim. Acta* **166**, 271–276 (2015).
26. Wang, L. et al. Electrochemical carbon monoxide reduction on polycrystalline copper: effects of potential, pressure, and pH on selectivity toward multicarbon and oxygenated products. *ACS Catal.* **8**, 7445–7454 (2018).
27. Lum, Y. W. & Ager, J. W. Stability of residual oxides in oxide-derived copper catalysts for electrochemical CO_2 reduction investigated with ^{18}O labeling. *Angew. Chem. Int. Ed.* **57**, 551–554 (2018).
28. Scott, S. B. et al. Absence of oxidized phases in Cu under CO reduction conditions. *ACS Energy Lett.* **4**, 803–804 (2019).
29. Luc W. et al. Two-dimensional copper nanosheets for electrochemical reduction of carbon monoxide to acetate. *Nat Catal.* **2**, 423–430 (2019).
30. Lum, Y. W., Cheng, T., Goddard, W. A. & Ager, J. W. Electrochemical CO reduction builds solvent water into oxygenate products. *J. Am. Chem. Soc.* **140**, 9337–9340 (2018).
31. Cheng, T., Xiao, H. & Goddard, W. A. Free-energy barriers and reaction mechanisms for the electrochemical reduction of CO on the Cu(100) surface, including multiple layers of explicit solvent at pH 0. *J. Phys. Chem. Lett.* **6**, 4767–4773 (2015).
32. Bagger, A., Arnarson, L., Hansen, M. H., Spohr, E. & Rossmeisl, J. Electrochemical CO reduction: a property of the electrochemical interface. *J. Am. Chem. Soc.* **141**, 1506–1514 (2019).
33. Calle-Vallejo, F. & Koper, M. T. M. Theoretical considerations on the electroreduction of CO to C_2 species on Cu(100) electrodes. *Angew. Chem. Int. Ed.* **52**, 7282–7285 (2013).
34. Feng, X. F., Jiang, K. L., Fan, S. S. & Kanan, M. W. A direct grain-boundary-activity correlation for CO electroreduction on Cu nanoparticles. *ACS Cent. Sci.* **2**, 169–174 (2016).
35. Dean J. A., Lange N. A. *Lange's Handbook of Chemistry* (McGraw-Hill, 1999).
36. Lundberg, H., Tinnis, F., Selander, N. & Adolfsson, H. Catalytic amide formation from non-activated carboxylic acids and amines. *Chem. Soc. Rev.* **43**, 2714–2742 (2014).
37. Watts, J. C. & Larson, P. A. "Dimethylacetamide" in *Kirk–Othmer Encyclopedia of Chemical Technology Online* (John C. Wiley & Sons, 2002). https://doi.org/10.1002/0471238961.0409130523012020.a01.pub2
38. McEnaney, J. M. et al. Ammonia synthesis from N_2 and H_2O using a lithium cycling electrification strategy at atmospheric pressure. *Energy Environ. Sci.* **10**, 1621–1630 (2017).
39. Jiao, F. & Xu, B. J. Electrochemical ammonia synthesis and ammonia fuel cells. *Adv. Mater.* **31**, 1805173 (2019).
40. Chen, J. G. et al. Beyond fossil fuel-driven nitrogen transformations. *Science* **360**, eaar6611 (2018).
41. Liu, K., Smith, W. A. & Burdyny, T. Introductory guide to assembling and operating gas diffusion electrodes for electrochemical CO reduction. *ACS Energy Lett.* **4**, 639–643 (2019).
42. Lu, X. & Zhao, C. Electrodeposition of hierarchically structured three-dimensional nickel–iron electrodes for efficient oxygen evolution at high current densities. *Nat. Commun.* **6**, 6616 (2015).
43. Luc, W., Jiang, Z., Chen, J. G. G. & Jiao, F. Role of surface oxophilicity in copper-catalyzed water dissociation. *ACS Catal.* **8**, 9327–9333 (2018).

Acknowledgements

F.J. would like to thank W. Luc for illustration assistance and E. Jeng for help with preparation of the anode. M.J. and J.-J.L. also thank B. Murphy and Z. J. Wang for help with GC–MS. The experimental work was financially supported by the US Department of Energy under award no. DE-FE0029868. F.J. also thanks the National Science Foundation Faculty Early Career Development program (award no. CBET-1350911). J.-J.L. acknowledges financial support from Chinese Scholarship Council. T.C. and W.A.G. were supported by the Joint Center for Artificial Photosynthesis, a DOE Energy Innovation Hub, supported through the Office of Science of the US Department of Energy under award no. DE-SC0004993. This work used the Extreme Science and Engineering Discovery Environment, which is supported by National Science Foundation grant no. ACI-1053575. This research used resources at the 8-ID Beamline of the National Synchrotron Light Source II, a US Department of Energy Office of Science User Facility operated by Brookhaven National Laboratory under contract no. DE-SC0012704. The authors acknowledge E. Stavitski (8-ID Beamline, NSLS-II, Brookhaven National Laboratory) for assistance in X-ray absorption spectroscopy measurements.

Author contributions

F.J. conceived the idea and supervised the project. M.J. and J.J.-L. performed the electrolysis experiments, analysed the data and wrote the first draft of the manuscript. B.H.K. performed the SEM characterization. T.C. and W.A.G. performed the computational modelling studies. All the authors contributed to the discussion of the results and preparation of the manuscript. M.J., J.J.L. and T.C. have the right to list themselves first in the bibliographic documents.

Competing interests

M.J., J.-J.L. and F.J. have filed a patent application (international patent application number: PCT/US 19/27012) that is based on the discovery presented in this work.

Additional information

Supplementary information is available for this paper at https://doi.org/10.1038/s41557-019-0312-z.

Reprints and permissions information is available at www.nature.com/reprints.

Correspondence and requests for materials should be addressed to W.A.G. or F.J.

Publisher's note: Springer Nature remains neutral with regard to jurisdictional claims in published maps and institutional affiliations.